

Compton Scattering and its Applications: The PLEIADES Femtosecond X-ray Source at Lawrence Livermore National Laboratory

*F. Hartemann, W. Brown, S.G. Anderson, C.P.J Barty, S.M. Betts
R. Booth, J.K. Crane, R.R. Cross, D.N. Fittinghoff, D.J. Gibson,
J. Kuba, B. Rupp, A.M. Tremaine, P.T. Springer*

U.S. Department of Energy

Lawrence
Livermore
National
Laboratory

This article was submitted to: International Workshop on Quantum Aspects
of Beam Physics, Hiroshima, Japan,
01/07/2003 - 10/2003

May 1, 2003

DISCLAIMER

This document was prepared as an account of work sponsored by an agency of the United States Government. Neither the United States Government nor the University of California nor any of their employees, makes any warranty, express or implied, or assumes any legal liability or responsibility for the accuracy, completeness, or usefulness of any information, apparatus, product, or process disclosed, or represents that its use would not infringe privately owned rights. Reference herein to any specific commercial product, process, or service by trade name, trademark, manufacturer, or otherwise, does not necessarily constitute or imply its endorsement, recommendation, or favoring by the United States Government or the University of California. The views and opinions of authors expressed herein do not necessarily state or reflect those of the United States Government or the University of California, and shall not be used for advertising or product endorsement purposes.

This is a preprint of a paper intended for publication in a journal or proceedings. Since changes may be made before publication, this preprint is made available with the understanding that it will not be cited or reproduced without the permission of the author.

This work was performed under the auspices of the United States Department of Energy by the University of California, Lawrence Livermore National Laboratory under contract No. W-7405-Eng-48.

This report has been reproduced directly from the best available copy.

Available electronically at <http://www.doc.gov/bridge>

Available for a processing fee to U.S. Department of Energy
And its contractors in paper from
U.S. Department of Energy
Office of Scientific and Technical Information
P.O. Box 62
Oak Ridge, TN 37831-0062
Telephone: (865) 576-8401
Facsimile: (865) 576-5728
E-mail: reports@adonis.osti.gov

Available for the sale to the public from
U.S. Department of Commerce
National Technical Information Service
5285 Port Royal Road
Springfield, VA 22161
Telephone: (800) 553-6847
Facsimile: (703) 605-6900
E-mail: orders@ntis.fedworld.gov
Online ordering: <http://www.ntis.gov/ordering.htm>

OR

Lawrence Livermore National Laboratory
Technical Information Department's Digital Library
<http://www.llnl.gov/tid/Library.html>

COMPTON SCATTERING AND ITS APPLICATIONS: THE PLEIADES FEMTOSECOND X-RAY SOURCE AT LLNL*

F.V. HARTEMANN, W.J. BROWN, S.G. ANDERSON, C.P.J. BARTY, S.M. BETTS, R.
BOOTH, J.K. CRANE, R.R. CROSS, D.N. FITTINGHOFF, D.J. GIBSON, J. KUBA, B.
RUPP, A.M. TREMAINE, AND P.T. SPRINGER

*Lawrence Livermore National Laboratory
7000 East Avenue,
Livermore, CA 94550, USA
E-mail: hartemann1@llnl.gov*

Remarkable developments in critical technologies including terawatt-class lasers using chirped-pulse amplification, high brightness photoinjectors, high-gradient accelerators, and superconducting linacs make it possible to design and operate compact, tunable, subpicosecond Compton scattering x-ray sources with a wide variety of applications. In such novel radiation sources, the collision between a femtosecond laser pulse and a low emittance relativistic electron bunch in a small (μm^3) interaction volume produces Doppler-upshifted scattered photons with unique characteristics: the energy is tunable in the 5-500 keV range, the angular divergence of the beam is small (mrad), and the pulses are ultrashort (10 fs – 10 ps). Two main paths are currently being followed in laboratories worldwide: high peak brightness, using ultrahigh intensity femtosecond lasers at modest repetition rates, and high average brightness, using superconducting linac and high average power laser technology at MHz repetition rates. Targeted applications range from x-ray protein crystallography and high contrast medical imaging to femtosecond pump-probe and diffraction experiments. More exotic uses of such sources include the γ - γ collider, NIF backlighting, nonlinear Compton scattering, and high-field QED. Theoretical considerations and experimental results will be discussed within this context.

1. Introduction

Remarkable advances in ultrashort pulse laser technology based on chirped-pulse amplification,¹⁻⁴ and the recent development of high-brightness, relativistic electron sources⁵⁻⁷ allow for the design of novel, compact, monochromatic, tunable, femtosecond x-ray sources using Compton scattering.⁸⁻²¹ Such new light sources are expected to have a major impact in a number of important fields of research, including the study of fast structural dynamics,²²⁻²⁵ advanced biomedical imaging,²⁶ and x-ray protein crystallography;^{27,28} however, the quality of both the electron and laser beams is of paramount importance in

* This work was performed under the auspices of the U.S. Department of Energy by the University of California, Lawrence Livermore National Laboratory under contract No. W-7405-Eng-48.

achieving the peak and average x-ray spectral brightness required for such applications.

In this paper, we describe the first production of x-rays using Compton scattering at Lawrence Livermore National Laboratory (LLNL). A brief summary of our main results is given here, while a more detailed description is provided in the remainder of the text. In January 2003, the PLEIADES (Picosecond Laser-Electron Inter-Action for the Dynamical Evaluation of Structures) facility produced first light at 70 keV. This important milestone offers a new opportunity to develop laser-driven, compact, tunable x-ray sources for critical applications such as NIF diagnostics and time-resolved material studies. Initial x-rays were captured with a cooled CCD using a Cesium Iodide scintillator; the peak photon energy was approximately 70 keV, and the observed angular distribution was found to agree very well with three-dimensional codes. The electron beam was focused to 80 μm rms, at 54 MeV, with 250 pC of charge, a relative energy spread of 0.2%, and a normalized emittance of 10 mm.mrad. Optimization of the x-ray dose is currently underway, with the goal of reaching 10^8 photons per shot and a peak brightness approaching 10^{20} photons/mm²/mrad²/s/0.1%bandwidth, which would represent a world-record brightness at this x-ray energy and pulse duration.

The aforementioned technical breakthroughs in the fields of solid-state lasers and high-brightness electron accelerators provide a unique opportunity to develop an entirely new class of advanced x-ray sources, with characteristics approaching those of third-generation light sources,²⁹ in a much more compact and inexpensive package. This, in turn, offers the possibility of an important spin-off of ultra-short pulse laser technology into the field of molecular biology, which is currently growing at an exponential rate: following the completion of the Human Genome Project,³⁰ the systematic study of protein structure and function^{31,32} is expected to dominate biophysics in the first half of the 21st Century. In addition, a new paradigm for rational drug design has now emerged, using both recombinant DNA technology³³ and x-ray protein crystallography. New classes of drugs,³⁴ as recently exemplified by the development of HIV protease inhibitors,^{35,36} successfully reduced the viral load of AIDS patients below the detection threshold of enzyme-linked immuno-sorbent assays.³⁷

In protein crystallography, recombinant DNA technology is used to produce large quantities of a given protein by splicing the corresponding coding DNA sequence into the genetic material of a bacterium. The transfected bacteria are cultivated and upon induction overexpress large quantities of the selected protein, which is then isolated, purified, and crystallized. Diffraction data are routinely collected at LN₂ temperature, and the experimental phase

measurements necessary for the reconstruction of the electron density are primarily determined by the multi-wavelength anomalous diffraction (MAD) method.^{27,28,38} Finally, a molecular model of the structure is built into the reconstructed three-dimensional electron density map.

The key characteristics of an x-ray source useful for protein crystallography are its small size, low angular divergence, good transverse coherence, and high average spectral brightness. In turn, these requirements determine the necessary electron and laser beam quality, as will be discussed extensively in this paper.

2. Electron Beam Design

PLEIADES (Picosecond Laser Electron Inter-Action for Dynamic Evaluation of Structures) is a next generation Compton scattering x-ray source being developed at LLNL. Ultra-fast ps x-rays (10-200 keV) will be generated by colliding an energetic electron beam (20-100 MeV) with a high intensity, sub-ps, 800 nm laser pulse. Generation of sub-ps pulses of hard x-rays (30 keV) has previously been demonstrated at the LBNL Advanced Light Source injector linac, with x-ray beam fluxes of 10^5 photons per pulse. The LLNL source is expected to achieve fluxes between $10^7 - 10^8$ photons for pulse durations of 100 fs to 5 ps using interaction geometries ranging from 90° (side-on collision) to 180° (head-on collision).

To achieve such a high x-ray flux, a very high brightness electron beam, capable of being focused to a 10-20 μm spot size at the interaction point, will be required. The PLEIADES beamline has been designed to meet these demands by producing a 1-2 ps, 500 pC bunch with a normalized emittance of less than 5 $\pi\text{mm-mrad}$.

2.1. Experimental Layout

The PLEIADES facility consists of a Ti-Sapphire laser system capable of producing bandwidth limited laser pulses of 50 fs with up to 1 joule of energy at 800 nm, an S-band photo-cathode RF gun, and a 100 MeV linac consisting of 4, 2.5-meter-long accelerator sections. The RF gun is driven by a picosecond, 1 mJ, UV laser that is synchronized to the interaction drive laser.

A schematic of the interaction region is shown in Figure 1. To maximize x-ray flux while minimizing effects of timing jitter, the laser incidence angle is currently 180 degrees with respect to the electron beam direction, though a 90 degree interaction geometry will also be possible. The focal length between the final focus quadrupole triplet and the interaction region is 10 cm to allow for maximum focus strength and minimum electron bunch spot size. A 30-degree

dipole magnet bends the electron bunch out of the x-ray beam path following the interaction. An off-axis, 1.5 m focal length parabolic mirror is used to focus the laser, which, assuming a diffraction limited spot, should reach a minimum spot size of about $15\ \mu\text{m}$ FWHM at the interaction point. Currently, a fused-silica flat mirror is placed in the x-ray beam path to serve as the final steering optic for the laser, though there are plans to replace this with a beryllium flat, which will be more transparent to the x-ray beam.

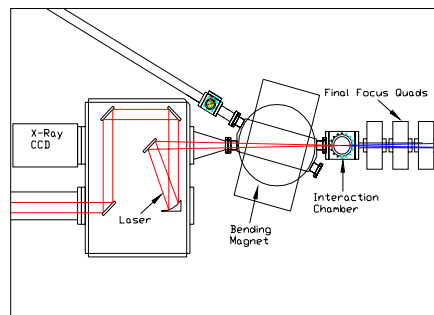


Figure 1. Interaction geometry.

2.2. *Electron beam production*

The electron beamline has been fully modeled, from the S-band photocathode RF gun to the interaction point using the Los Alamos particle dynamics code, PARMELA, and the electro-static and electromagnetic field solvers: POISSON and SUPERFISH. These include simulations of emittance compensation between the RF gun and the first linac section, velocity compression of the bunch through the first linac section, and subsequent acceleration and optimization of beam energy spread and emittance during transport through the subsequent accelerator sections.

The two primary factors that determine the minimum electron bunch spot size at the interaction point are beam emittance and energy spread. In addition, the x-ray flux will also depend on electron bunch charge. However, optimizing emittance and energy spread places a practical limit on the amount of charge in the bunch. After finding optimized cases for several different bunch charges, 0.5 nC was found to be a good compromise between high bunch charge and low emittance.

The RF gun is designed to accelerate an electron bunch to an initial energy of 5 MeV, with a peak accelerating gradient of 110 MV/m. The beam is transported

to the first linac section, during which emittance compensation is performed by focusing the beam to a waist with a solenoid placed directly after the RF gun.

Two modes of linac operation have been investigated through simulation. The first case is when the electron beam is accelerated on crest through the accelerator. In this case, the minimum electron bunch length is about 6 ps FWHM. The second mode of operation employs velocity compression, in which the beam is injected near the zero crossing of the accelerating field in order to provide an energy chirp to the beam, resulting in compression of the accelerated bunch. The second accelerator section is then used to accelerate the beam from about 10 MeV to about 35 MeV. The third and fourth sections can then be used to either remove a large portion of the energy spread induced by the velocity compression process, or to simply accelerate the beam further, depending on the final beam energy desired. Throughout the acceleration process, the linac solenoids are carefully optimized to minimize emittance growth.

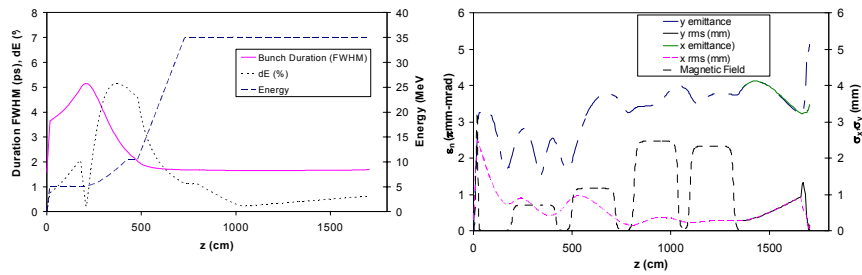


Figure 2. PARMELA simulation showing electron bunch parameters (energy, energy spread, and bunch length) versus longitudinal position in the beam line. The gun cathode position corresponds to $z = 0$ cm, while the interaction region is located at $z = 1700$ cm.

Figure 3. PARMELA simulation showing electron bunch parameters (emittance, and spot size) versus longitudinal position in the beam line. The dotted line shows the solenoid magnetic field strength (in kG) for the gun solenoid and the four linac solenoids.

Figures 2 and 3 show the evolution of several of the beam characteristics during the acceleration process determined from PARMELA simulations, including emittance, energy spread, and bunch length. Velocity compression is used to reduce the rms bunch length from about 2.5 ps at the entrance of the accelerator to about 0.7 ps at its exit. While it is possible to compress further, this bunch length was chosen to minimize emittance growth resulting from the compression process, while maximizing x-ray yield from the Compton scattering interaction. By not compressing fully, it is also possible to remove more of the energy spread in the bunch by accelerating off crest in subsequent accelerator

sections. This is performed by accelerating the bunch at the opposite zero crossing (180 degree shift) of the zero crossing used in first accelerator section to compress the beam. At the exit of the linac, the bunch energy spread has been reduced to 0.5 % rms, while the rms normalized emittance is 3.5π mm-mrad. In this particular case, the final electron beam energy is 35 MeV, though it is possible to obtain larger beam energies (up to 100 MeV) with similar results.

Final focus simulations were performed using PARMELA and Trace-3D. The electrons are transported 3 meters from the accelerator exit and focused with a quadrupole triplet. The triplet is about 50 cm long, and the focal length is about 10 cm. The maximum field gradient in the quadrupole magnets is 15 T/m. The rms convergence angle of the focus is about 3 mrad. In the simulation, the beam is initially defocused in y , leading to a larger size in this dimension going into the second quadrupole. This results in more significant chromatic aberrations in the y dimension than in x , and is manifested by a slightly larger emittance and spot size in y at the interaction point, as can be seen in PARMELA simulations of the final focus. Figure 4 shows the transverse profile of the electron bunch at the focus as determined by PARMELA. The electron beam focus parameters are summarized in Table 1.

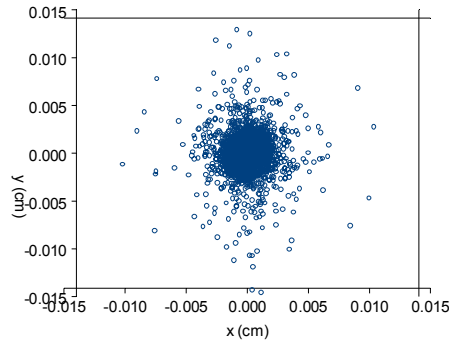


Figure 4. Profile of the electron beam at focus.

TABLE 1. Electron Beam Parameters at Focus.

Parameter	Value
ε_{xn} (mm-mrad)	3.4
ε_{yn} (mm-mrad)	5.0
σ_x (μm)	12
σ_y (μm)	20
σ_t (ps)	0.74

3. Calculation of X-ray Production

The expected x-ray production was calculated and the effects of RF phase and timing jitter were determined by integrating the emission probability per unit time, dN_x/dt , given by

$$\frac{dN_x}{dt}(t) = \sigma c [1 - \mathbf{v} \cdot \mathbf{k}] \iiint n_\gamma(\mathbf{x}, t) n_e(\mathbf{x}, t) d^3x, \quad (1)$$

where N_x is the total number of x-rays produced, $n_\gamma(\mathbf{x}, t)$ is the laser photon density, $n_e(\mathbf{x}, t)$ is the electron density, σ is total Compton cross section, \mathbf{v} is the velocity of the electron beam, and \mathbf{k} is the wave number of the laser pulse. The calculations were performed for a 300 mJ, 300 fs laser pulse in conjunction with the PARMELA output in place of $n_e(\mathbf{x}, t)$. In this case, $n_\gamma(\mathbf{x}, t)$ was assumed to have a Gaussian profile, given by

$$n_\gamma(r, z, t) = \frac{\eta_\gamma}{1 + (z/z_0)^2} \exp\left[-2\left(\frac{t - z/c}{\Delta t}\right)^2\right] \exp\left\{-\frac{2r^2}{w_0^2 [1 + (z/z_0)^2]}\right\}, \quad (2)$$

where z_0 is the laser Rayleigh length, Δt is the pulse duration, η_γ is the peak photon density, and w_0 is the minimum laser spot size. $n_e(\mathbf{x}, t)$ is replaced with a delta-function representing the position and charge of each PARMELA macro-particle as a function of time. Figure 5 shows the calculated x-ray pulse profile in time. The average photon energy is 30 keV, and the peak x-ray flux is about 6×10^{19} photons/s with an integrated photon yield of about 10^8 . A 3-D frequency domain calculation of the x-ray output has also been performed, showing the on axis spectral bandwidth to be about 10%. The peak spectral brightness is calculated to be 10^{20} photons/s/0.1% bandwidth/mm²/mrad².

Effects of phase jitter were simulated by varying the relative phase of the linac sections with respect to the RF gun in the PARMELA simulations, and using the resulting electron beam parameters in the calculation of the x-ray production. Figure 6 shows the expected x-ray yield versus phase jitter for the cases where the electron beam is compressed in the first section (accelerated near the zero crossing), and not compressed (accelerated on crest).

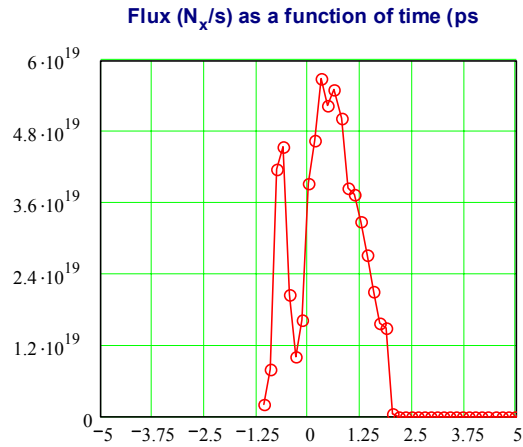


Figure 5. X-ray flux (photon/s) vs. time (ps). The total number of photons in the pulse is about 10^8 , and the average photon energy is 30kV.

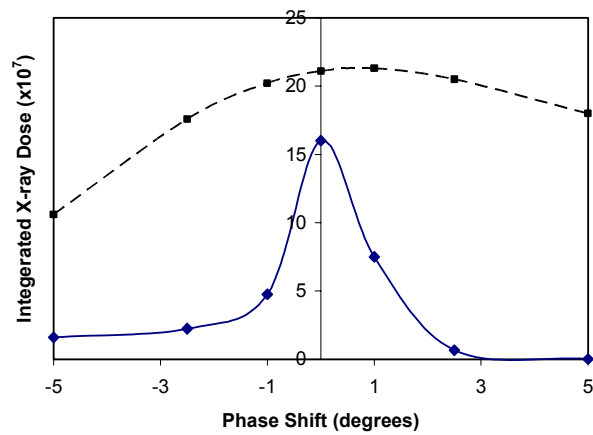


Figure 6. Simulated x-ray yield versus phase shift (Solid: compressed beam. Dotted: uncompressed).

It is seen that the phase jitter requirement for the compressed beam is less than one degree (or about 1 ps). Thus, picosecond phase and timing control will be required to maintain stability of the x-ray source when velocity compression is implemented.

4. Electron Beam Characterization

To date, electron bunches with up to 700 pC of charge have been produced with up to 100 μ J of UV laser energy incident on the gun photo-cathode. The beam has been transported through the linac and accelerated up to 60 MeV. Quad scan emittance measurements have been performed for 300 pC, 60 MeV bunches, yielding a normalized rms emittance of 9 mm-mrad (Figure 7). The rms energy spread has been measured to be 0.2%. Improvements in emittance are expected with improvements in the UV drive laser uniformity and optimization of the electron beam transport. Additionally, an increased gradient in the RF gun will help improve the emittance. A new cathode has been installed in hopes of alleviating breakdown problems that have limited the accelerating gradient to about 80 MV/m.

Phase jitter between the drive laser oscillator and the RF phase in the gun has been measured by mixing a 2.8 GHz signal generated by the laser oscillator with a signal produced by a probe inside the RF gun. This has shown short time scale (< 1 minute) phase stability of ± 1 degree. Longer term phase drifts are mitigated by a computer controlled feed back loop and voltage controlled phase shifter. Plans are also underway to implement a direct measurement of the UV drive laser arrival phase in the RF gun. The direct phase measurement will employ a 20 GHz bandwidth, 800 nm optical fiber switch modulated by microwaves sampled from the RF gun to provide a nonlinear correlation between the gun fields and the IR laser pulse used to produce the UV photocathode drive laser.

Both the electron beam and the interaction drive laser have been imaged by placing a metal cube in at the interaction point to send OTR light from the electron beam and laser light into the same camera. Using a CCD camera, the electron beam spot sized has been measured to be about 70 μ m rms, while the laser spot size has been measured to be about 30 μ m. This is about twice the optimized spot sized determined from PARMELA simulations, based on the measured beam emittance. Further optimization of the final focus quads should help reduce the spot size.

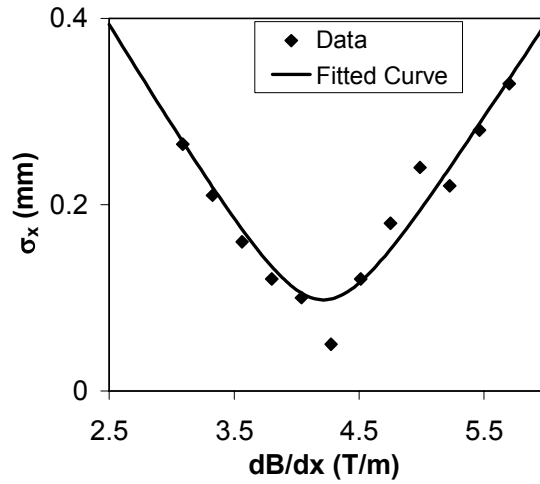


Figure 7. Quadrupole scan measurement of 60 MeV, 300 pC electron beam. $\epsilon_n = 9.3 \pi \text{mm-mrad}$.

The synchronization and timing overlap between the laser and electron bunches have been performed with a streak camera. A schematic of the measurement, as well as the streak camera image is shown in Figure 8, indicating good temporal overlap of the two bunches. The jitter has been measured to be within the resolution of the streak camera (about 2 ps). Additionally, indirect timing jitter measurements performed by mixing wakefields produced by the electron bunch with a frequency multiplied photo-diode signal from the laser oscillator are consistent with the jitter results obtained by the streak camera measurements, indicating an rms timing jitter less than 2 ps.

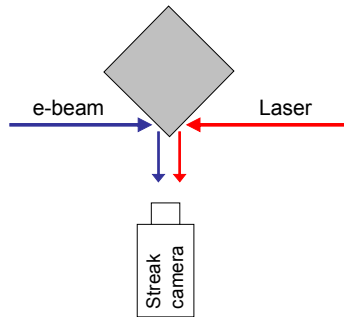


Figure 8. E-beam to laser synchronization measurement.

5. X-Ray Production

First light of the PLEIADES Thomson x-ray source has been achieved. Figure 9 shows the measured beam profile taken with the x-ray CCD camera. The electron beam energy in this case was 60 MeV, and the bunch charge was about 300 pC. Due to the optical misalignments, which have since been corrected, the laser energy delivered at the interaction was only about 40 mJ. The image is integrated over 1200 shots. The estimated average photon count per shot at the interaction point is about 5×10^4 , and the peak photon energy is about 70 keV. The theoretical intensity profile (shown on the right hand side of Figure 9) agrees well with the measured profile. The theoretical curve includes the broadening effects of the measured beam emittance as well as the narrowing effect derived from the spectral dependence of the x-ray transmission coefficient through the laser turning mirror.

Dramatic improvements of the per shot x-ray dose are expected after improvement in the electron beam final focus, reduction of electron beam emittance through the optimization of the photocathode UV drive laser profile and electron beam transport optics, and the optimization of the IR drive laser energy delivered to the interaction region. This will allow for the realization of final focus spot sizes as small as $10 \mu\text{m}$ rms, enabling the production of up to 10^8 x-ray photons per collision.

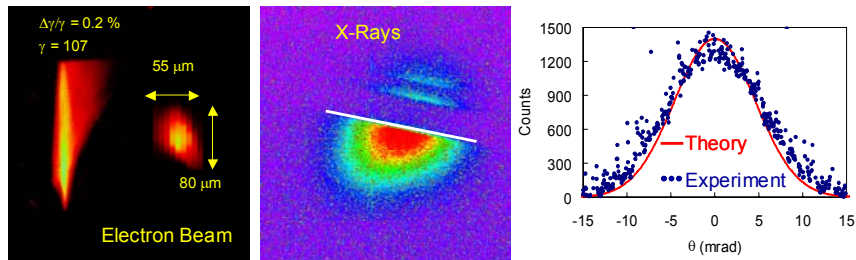


Figure 9. Measurement of X-ray beam profile. Left: CCD image. Right: Lineout intensity profile: measurement (dots), theory (line).

6. Conclusions

The PLEIADES Thomson X-ray source is a unique, high peak brightness x-ray source that, when optimized, will be useful for ultra-fast imaging applications to temporally resolve material structural dynamics on atomic time scales. Electron beam simulations and x-ray production codes have been

performed to completely model the theoretical source performance. To date, 0.3 nC, 60 MeV bunch had been focused to 70 μm rms spot sized and collided with a 40 mJ, 30 μm laser pulse to produce 70 keV x-rays. Optimization of the experiment will include increasing the laser energy delivered to the interaction region to about 300 mJ, and decreasing the electron beam emittance to less the 5 mm-mrad rms. This will enable the achievement of a 10 μm spot size at the interaction and the production of 10^8 x-ray photons per pulse. Once optimization is complete, PLEIADES should achieve a peak x-ray brightness approaching 10^{20} photons/0.1% bandwidth/ $\text{mm}^2/\text{mrad}^2$.

The PLEIADES Compton x-ray source facility will provide high brightness ($> 10^7$ x-rays/pulse), picosecond pulses for dynamic measurements in matter, including radiography, dynamic diffraction, and spectroscopy. The PLEIADES electron beamline will be capable of producing the high brightness electron beam needed to drive this source. Simulations have shown that a 1 ps, 500 pC bunch with an rms normalized emittance of less than 5 $\pi\text{mm-mrad}$ should be achievable, and will allow for the attainment of a 10 μm rms spot size at the interaction point. Initial electron beam measurements have been performed, and expected performance parameters and planned jitter measurements and control methods have been presented.

References

1. M.D. Perry and G. Mourou, *Science* **264** (5161), 917-924 (1994).
2. G.A. Mourou, C.P.J. Barty, and M.D. Perry, *Phys. Today* **51** (1), 22-28 (1998).
3. C.P.J. Barty, *et al.*, *Opt. Lett.* **21**, 668 (1996).
4. D.P. Umstadter, C. Barty, M. Perry, and G.A. Mourou, *Opt. Phot. News* 9 (1), 41 (1998).
5. *Advanced Accelerator Concepts, 8th Workshop*, edited by W. Lawson, C. Bellamy, and D.F. Brosius, American Institute of Physics, Conference Proceedings No. 472, Woodbury, NY, 1999.
6. D. Yu *et al.*, *Proc. Particle Accelerator Conference 1999, 2003* (1999).
7. S.G. Biedron, *et al.*, *Proc. Particle Accelerator Conference 1999, 2024* (1999).
8. R.W. Schoenlein, *et al.*, *Science* **274** (5285), 236-238 (1996).
9. W.P. Leemans, *et al.*, *Phys. Rev. Lett.* **77**, 4182 (1996).
10. W.P. Leemans, *et al.*, *IEEE J. Quantum Electron.* **QE11**, 1925 (1997).
11. C. Bula, *et al.*, *Phys. Rev. Lett.* **76**, 3116 (1996).
12. D. Burke, *et al.*, *Phys. Rev. Lett.* **79**, 1626 (1997).
13. C. Bamber, *et al.*, *Phys. Rev.* **D60** (9), 092004/1-43 (1999).
14. V.N. Litvinenko, *et al.*, *Phys. Rev. Lett.* **78**, 4569 (1997).

15. W. Greiner and J. Reinhardt, *Quantum Electrodynamics*, Springer-Verlag, Berlin, 1994, Chap. 3.7.
16. E. Esarey, S.K. Ride, and P. Sprangle, Phys. Rev. **E48**, 3003-3021 (1993).
17. F.V. Hartemann, *et al.*, Phys. Rev. **E54**, 2956-2962 (1996).
18. S.K. Ride, E. Esarey, and M. Baine, Phys. Rev. **E52**, 5425-5442 (1995).
19. E. Esarey, P. Sprangle, and J. Krall, Phys. Rev. **E52**, 5443-5453 (1995).
20. F.V. Hartemann and A.K. Kerman, Phys. Rev. Lett. **76**, 624-627 (1996).
21. F.V. Hartemann, Phys. Plasmas **5**, 2037-2047 (1998).
22. C.W. Siders, *et al.*, Science **286** (5443), 1340 (1999); C. Rose-Petruck, *et al.*, Nature **398**, 310 (1999).
23. A.H. Chin, *et al.*, Phys. Rev. Lett. **83**, 336 (1999).
24. A.M. Lindenberg, *et al.*, Phys. Rev. Lett. **84**, 111 (2000).
25. R.A. Robb, *Three-Dimensional Biomedical Imaging: Principles and Practice*, Wiley-VCH Publishers, New York, NY, 1995.
26. R. Fitzgerald, Phys. Today **53** (7), 23 (2000).
27. J. Drenth, *Principles of Protein X-Ray Crystallography*, 2nd Ed., Springer-Verlag, New York, NY, 1999.
28. K.E. van Holde, W. Curtis Johnson, and P. Shing Ho, *Principles of Physical Biochemistry*, Prentice-Hall, Inc., Upper Saddle River, NJ, 1988, Chap. 6.
29. D. Atwood, *Soft X-Rays and Extreme Ultraviolet Radiation*, Cambridge University Press, Cambridge, U.K., 1999.
30. F. Golden and M.D. Lemonick, Time **156** (1), 19 (2000).
31. K. Garber, Tech. Rev. **103** (4), 46-56 (2000).
32. M.D. Lemonick, Times **156** (1), 24 (2000).
33. B.D. Hames, N.M. Hooper, and J.D. Houghton, *Biochemistry*, Springer, New York, NY, 1997, Sec. I.
34. M. Balter, Science **274** (5295), 1988 (1996).
35. *Nucleic Acids in Chemistry and Biology*, 2nd Ed., Edited by G. M. Blackburn and M.J. Gait, Oxford University Press, New York, NY, 1996.
36. L. Montagnier, *Virus*, W.W. Norton & Co., New York, NY, 2000.
37. J. Nicklin, K. Graeme-Cook, T. Paget, and R. Killington, *Microbiology*, Springer, New York, NY, 1999, Sec. K.; P.C. Turner, A.G. McLenna, A.D. Bates, and M.R.H. White, *Molecular Biology*, Springer, New York, NY, 1998, Secs. R and S.
38. W.A. Hendrickson and C.M. Ogata, Methods Enzymol., **276**, 494-516 (1997).
39. P.A.M. Dirac, Proc. R. Soc. London, Ser. **A167**, 148 (1938).
40. F.V. Hartemann, *et al.*, Phys. Rev. **E58**, 5001-5012 (1998).
41. B. Quesnel and P. Mora, Phys. Rev. **E58**, 3719-3732 (1998).
42. F.V. Hartemann, Phys. Rev. **E61**, 972-975 (2000).
43. M.J. Hogan, *et al.*, Phys. Rev. Lett., **81**, 4867-4870 (1998).
44. M. Reiser, *Theory and Design of Charged Particle Beams*, John Wiley and Sons, New York, NY, 1994, Chaps. 3 and 6.

45. H. Wiedemann, *Particle Accelerator Physics*, Vol. 1, 2nd Ed., Springer, New York, NY, 1999, Chaps. 5 and 8.
46. B.E. Carlsten, Nucl. Instrum. Methods Phys. Res. **A285**, 313-319 (1989).
47. W. Pauli, *Theory of Relativity*, Dover, New York, NY, 1958, Secs. 19, 27, 28.
48. R.P. Feynman, R.B. Leighton, and M. Sands, *The Feynman Lectures on Physics*, Vol. 2, Addison-Wesley, Reading, MA, 1964, Chap. 25.
49. H. Goldstein, *Classical Mechanics*, 2nd Ed., Addison-Wesley, Reading, MA, 1980.
50. A.O. Barut, *Electrodynamics and Classical Theory of Fields and Particles*, Dover, New York, NY, 1980, Chaps. 3 and 5.
51. J.D. Jackson, *Classical Electrodynamics*, 2nd Ed., John Wiley and Sons, New York, NY, 1975, Chap. 14.
52. C.W. Roberson and P. Sprangle, Phys. Fluids **B1**, 3 (1989)
53. I.S. Gradshteyn and I.M. Ryzhik, *Table of Integrals, Series, and Products*, 4th Ed., Academic Press, Orlando, FL, 1980, Eqs. 3.923, 3.924, and 3.323.3.
54. A.D. Yeremian, private communication (2000).
55. S. Wolfram, *The Mathematica Book*, 3rd Ed., Wolfram Media, Champaign, IL, 1996.
56. Los Alamos Accelerator Code Group, *Computer Codes for Particle Accelerators Design and Analysis: a Compendium*, 2nd Ed., LANL, Los Alamos, NM, 1990.
57. E. Jabri, *et al.*, Science **68** (2), 998-1004 (1995).
58. W.A. Hendrickson, *et al.*, D. M. Embo. J. **5**, 1665-72 (1990).
59. W.P. Burmeister, Acta Cryst. **D56**, 328-341 (2000).
60. M. Hart and L. Berman, Acta Cryst. **A54**, 850-858 (1998).
61. L.C. Jiang, B. Verman, and K.D. Joensen, J. Appl. Cryst. **33** (1), 801-803 (2000).
62. S. Ringhofer, R. Ulrich, B.Segelke, M.Knapp, B.Rupp. ACA Golden Anniversary Meeting, July 22-27, 2000, St. Paul, MN. ACA Meeting Series **27**, 111.
63. Brent W. Segelke, M. Forstner, M.Knapp. S.Trakhanov, S.Parkin, Y.Newhouse, H.D.Bellamy, K.H.Weisgraber and B.Rupp, Protein Science **9** (5), 886 - 897 (2000).
64. A web-based introduction into protein crystallography, including MAD phasing techniques, can be found at: <http://www-structure.llnl.gov/Xray/101index.html>
65. S.y. Chen, A. Maksimchuk, and D. Umstadter, Nature **396** (12), 653 (1998).
66. Handbook of Mathematical Functions, Edited by M. Abramowitz and I.A. Stegun, Dover, New York, NY, 1965, Chap. 13.
67. A. M. Weiner, *et al.*, J. Opt. Soc. Am. **B5**, 1563 (1988).
68. F. Rohrlich, *Classical Charged Particles*, Addison-Wesley, Reading, MA, 1965, Chaps. 6 and 9.